Sphinx Journal of Mathematical Sciences
1(2), 56–71, 2026
DOI:https://doi.org/10.64389/sjms.2026.012119
https://sphinxsp.org/journal/index.php/sjms/

Research article

Axisymmetric Thermal Response of a Nonlocal Visco-Thermoelastic Medium under MGT Heat Conduction with HTT and Fractional-Order Effects

Saurav Sharma[1,*], **Ravinder Kumar**[2]

[1] 1277 Harrow Cres, Yardley, Pennsylvania-19067 USA

[2] Department of Mathematics, Ch.Devi University, Sirsa, Haryana, India

* **Correspondence:** sauravkuk@gmail.com

ARTICLE INFO

Keywords:
Moore-Gibson-Thompson heat equation;
visco-thermoelasticity;
hyperbolic two-temperature;
nonlocal theory;
fractional-order derivative;
circular thermal source

Mathematics Subject Classification:
74A15, 74A18.

Important Dates:
Received: 16 May 2026
Revised: 12 June 2026
Accepted: 14 June 2026
Online: 17 June 2026

ABSTRACT

This paper investigates a two-dimensional axisymmetric thermal source problem in a homogeneous and isotropic visco-thermoelastic half-space governed by the Moore-Gibson-Thompson (MGT) heat equation. The model includes nonlocal effects, hyperbolic two-temperature (HTT) theory, viscosity and fractional-order derivative (FOD) effects. A circular thermal source is prescribed on the bounding plane, while the surface is assumed to be mechanically traction-free. The governing equations are written in nondimensional form and reduced by introducing suitable potential functions. The Laplace transform with respect to time and the Hankel transform with respect to the radial coordinate are applied to obtain the transformed expressions for the displacement components, stress components, conductive temperature and thermodynamic temperature. The transformed solutions are inverted numerically to study the effect of the nonlocal parameter, HTT parameter, viscosity and fractional-order parameter on the field quantities generated by the circular thermal loading. The numerical results show that these parameters have a clear influence on the normal stress, tangential stress, conductive temperature and temperature distribution. Several limiting cases are also obtained, which confirms the generality of the present formulation.

1. Introduction

Thermoelasticity describes the coupled interaction between deformation and temperature fields and provides a fundamental theoretical framework for analyzing solids subjected to simultaneous mechanical and thermal disturbances. In classical thermoelasticity, heat propagation is governed by Fourier's law, which implies an infinite speed of thermal signals. This prediction is physically unrealistic for transient thermal processes, especially in advanced materials subjected to rapid thermal loading. To overcome this limitation, Lord and Shulman [14] proposed a generalized dynamical theory of solids by introducing a single thermal relaxation time into the heat-conduction equation. Green and Lindsay [12] developed another generalized thermoelastic model by incorporating relaxation parameters into the constitutive relations. These generalized theories established the foundation for finite-speed thermal-wave propagation and more realistic thermo-mechanical coupling.

The two-temperature theory represents an important refinement of generalized thermoelasticity because it distinguishes between the conductive temperature and the thermodynamic temperature. Chen and Gurtin [5] introduced a theory of heat conduction involving two temperatures, and Chen et al. [6] extended this concept to thermoelastic materials. Youssef [25] later developed the theory of two-temperature generalized thermoelasticity, while Youssef and El-Bary [26] formulated a hyperbolic two-temperature generalized thermoelasticity theory. These models are particularly useful for studying transient thermal interactions in materials where the classical single-temperature description is insufficient.

Several studies have applied generalized thermoelasticity and hyperbolic two-temperature theory to different physical and engineering problems. Alzahrani and Abbas [4] investigated photo-thermal interactions in a semiconducting medium with a spherical cavity under the hyperbolic two-temperature model. Youssef et al. [27] analyzed thermal stresses in a damaged solid sphere using hyperbolic two-temperature generalized thermoelasticity theory. El-Bary [8] applied the diagonalization method to a hyperbolic two-temperature generalized thermoelastic solid sphere under mechanical damage effects. These studies demonstrate the importance of hyperbolic two-temperature models in describing thermoelastic behavior in spherical, semiconducting and damaged solid media.

For micro- and nano-scale structures, classical continuum theory may become inadequate because size-dependent effects can significantly influence the mechanical and thermal response. Nonlocal continuum theory addresses this limitation by allowing the stress at a point to depend not only on the local strain but also on the strain field in the surrounding region. Eringen and Edelen [9] introduced the theory of nonlocal elasticity, which has become an important framework for small-scale structural problems. Yu et al. [28] developed nonlocal thermoelasticity by combining nonlocal elasticity with nonlocal heat conduction. Abouelregal [1] proposed a nonlocal thermoelastic model involving higher-order time derivatives, while Saeed and Abbas [20] investigated the effects of nonlocal thermoelasticity in nanoscale thermoelastic materials. These contributions indicate that nonlocal parameters are essential for accurately modeling thermo-mechanical behavior at small length scales.

In recent years, the Moore-Gibson-Thompson heat equation has attracted considerable attention because it introduces a higher-order thermal relaxation mechanism and improves the description of heat transfer in generalized thermoelastic media. Quintanilla [19] formulated thermoelasticity within the Moore-Gibson-Thompson framework. Marin et al. [17] obtained results in the Moore-Gibson-Thompson thermoelasticity theory of dipolar bodies. Abouelregal et al. [2] analyzed a viscoelastic stressed microbeam subjected to laser excitation using the Moore-Gibson-Thompson heat equation on a Winkler foundation. Abouelregal et al. [3] further studied magneto-thermoelastic interactions in an orthotropic viscoelastic solid under the Hall current effect using a fourth-order Moore-Gibson-Thompson equation. These studies show that the Moore-Gibson-Thompson model provides a useful and physically meaningful extension of generalized thermoelasticity for complex materials and coupled-field problems.

Viscoelasticity is another important feature in the analysis of advanced materials because many solids, polymers, biological tissues and composites exhibit time-dependent deformation under dynamic thermal and mechanical loading. Ezzat et al. [11] studied relaxation effects associated with the volume properties of viscoelastic materials in generalized thermoelasticity with thermal relaxation. Ezzat et al. [10] introduced fractional calculus into one-dimensional isotropic thermo-viscoelasticity. Fractional-order models are particularly useful for describing memory-dependent material behavior, since they provide a flexible way to capture hereditary effects in thermo-mechanical processes.

Axisymmetric thermoelastic problems are important for spherical, cylindrical, layered and radially loaded structures, where the deformation and temperature fields vary with radial position. Miglani and Kaushal [18] investigated axisymmetric deformation in generalized thermoelasticity with two temperatures. Dhaliwal and Singh [7] provided a detailed treatment of dynamic coupled thermoelasticity, which remains a useful foundation for analyzing coupled thermal and elastic wave propagation. In broader coupled-field applications, Sharma and Khator [23] studied power-generation planning with reserve dispatch and weather uncertainties, while Sharma and Khator [24] examined micro-grid planning in a renewable-inclusive prosumer market. Although these works are from energy-system modeling, they reflect the wider importance of coupled physical processes in modern engineering systems.

Recent studies have further extended thermoelastic modeling by incorporating micropolar, photothermal, piezo-photothermal, fractional, nonlocal, phase-lag and semiconductor effects. Sharma [21] examined the effect of the impedance limit on plane-wave reflection in a micropolar thermoviscoelastic material using a modified Green-Lindsay model. Lotfy et al. [16] studied piezo-photothermal wave dynamics in an orthotropic hygrothermal semiconductor exposed to heat and moisture flux. Lotfy et al. [15] investigated fractional photo-thermoelastic waves in hydrodynamic semiconductors with Hall currents and variable thermal conductivity. Hilal et al. [13] analyzed thermomechanical waves in a magnetized microelongated thermoelastic medium using the Moore-Gibson-Thompson model. Sharma (2025) developed fundamental solutions and Green's functions for orthotropic photothermoelastic diffusion media under the Moore–Gibson–Thompson model, providing a useful analytical framework for studying coupled thermoelastic, diffusion and semiconductor-related field quantities [22].

Motivated by these developments, the present study investigates a two-dimensional axisymmetric thermoelastic problem within the Moore-Gibson-Thompson framework by incorporating fractional-order viscoelasticity, nonlocal parameters and hyperbolic two-temperature effects. The governing field equations and constitutive relations are formulated in the absence of body forces and heat sources and are expressed using suitable potential functions. The Laplace transform is applied in the time domain, while the Hankel transform is employed with respect to the radial coordinate to obtain the general solution in the transformed domain. The transformed expressions are evaluated under appropriate boundary conditions, and numerical results are presented graphically to examine the influence of viscosity, fractional-order parameters, hyperbolic two-temperature parameters and nonlocal effects on the thermo-mechanical response of the medium.

The novelty of the present work lies in the unified treatment of fractional-order viscoelasticity, nonlocal thermoelasticity and hyperbolic two-temperature effects within an axisymmetric Moore-Gibson-Thompson thermoelastic model. This combined framework provides a refined and physically meaningful approach for analyzing advanced materials and structures subjected to coupled thermal and mechanical loading conditions.

2. CONSTITUTIVE RELATIONS AND BASIC EQUATIONS

Following the formulations of Quintanilla [19], Eringen [9], and Ezzat et al. [11], the governing field equations and constitutive relations are developed in the absence of body forces and heat sources and are expressed as follows.

$$(\lambda_0 + \mu_0)\,\nabla\left(\nabla\cdot\vec{u}\right) + \mu\nabla^2\vec{u} - \beta_1\nabla T = \rho\left(1-\xi_1^2\nabla^2\right)\frac{\partial^2\vec{u}}{\partial t^2}, \tag{2.1}$$

$$\left(1+\frac{\tau_0^\alpha}{\alpha!}\frac{\partial^\alpha}{\partial t^\alpha}\right)\left[\rho C_e\ddot{T}+\beta_1T_0\ddot{e}\right] = K^*\nabla^2\dot{\phi}+K_1\nabla^2\phi, \tag{2.2}$$

$$t_{ij} = \lambda u_{k,k}\delta_{ij} + \mu\left(u_{i,j}+u_{j,i}\right) - \beta_1 T\delta_{ij}, \tag{2.3}$$

$$\ddot{\phi} - \ddot{T} = \beta^*\nabla^2\phi. \tag{2.4}$$

where

$$T = \left(1 - a\nabla^2\right)\phi,$$

$$\lambda_0 = \lambda\left(1+Q_1\frac{\partial}{\partial t}\right), \qquad \mu_0 = \mu\left(1+Q_2\frac{\partial}{\partial t}\right),$$

where $(Q_1, Q_2) = \left(\frac{\lambda^v}{\lambda}, \frac{\mu^v}{\mu}\right)$ being viscoelastic relaxation times; λ_v, μ_v – viscoelastic constants; λ, μ – Lamé's constants; $\mathbf{u}$ – displacement vector; $\beta_1 = (3\lambda + 2\mu)\alpha_t$; α_t – coefficient of linear thermal expansion; ξ_1 – non-local parameter; t_{ij} – components of stress tensor; t – time; ρ, C_e – density and specific heat respectively; K^* – thermal conductivity; $K_1 = (\lambda + 2\mu)/(4C_e)$ – material constant; ∇^2 – Laplacian operator; ϕ – conductive temperature; T – thermodynamic temperature; a – two temperature parameter; $\tau_0^\alpha \equiv \tau_0, \tau_1$ – relaxation time; δ_{ij} – Kronecker's delta; β^* – hyperbolic two temperature parameters; α – fractional parameter.

The equations (2.1), (2.2), (2.3), and (2.4) reduces to the following cases

Coupled theory of thermoelectricity (1980): $K^* = \tau_0^\alpha = 0.$

Lord Shulman Model (1962) (LS model): $K^* = 0,\ \tau_0^\alpha \neq 0.$

Green-Naghdi-II model (1992) (GN-II model): $K = 0,\ K_1^* \neq 0,\ \tau_0^\alpha = 0.$

Green-Naghdi-III model (1993) (GN-III model): $K \neq 0,\ K_1^* \neq 0,\ \tau_0^\alpha = 0.$

3. FORMULATION AND SOLUTION OF THE PROBLEM

An axisymmetric thermal source problem is considered for a homogeneous and isotropic visco-thermoelastic half-space $z \geq 0$, whose plane boundary $z = 0$ is subjected to a prescribed circular thermal source. The response is modeled within the Moore-Gibson-Thompson (MGT) heat-conduction framework by incorporating nonlocality, hyperbolic two-temperature (HTT) effects, viscosity and fractional-order derivative (FOD) effects.

A cylindrical polar coordinate system (r, θ, z) is used, with the origin on the bounding plane and the positive z-axis directed into the medium. Owing to axisymmetry, all field variables are independent of θ, and the displacement field is taken as

$$\overset{r}{u} = (u_r,\ 0,\ u_z) \tag{3.1}$$

We now define dimensionless quantities as:

$$\left(r', z', u_r', u_z', \xi_1'\right) = \frac{\omega_1}{c_1}\left(r, z, u_r, u_z, \xi_1\right), \quad \left(t_{zz}', t_{zr}', F_1'\right) = \frac{1}{\beta_1 T_0}\left(t_{zz}, t_{zr}, F_1\right),$$

$$\left(\phi', T'\right) = \frac{1}{T_0}\left(\phi, T\right), \quad a' = \frac{\omega_1^2}{c_1^2}a, \quad \beta^{*'} = \frac{1}{c_1^2}\beta^*, \quad \left(t', \tau_0'\right) = \omega_1\left(t, \tau_0\right), \tag{3.2}$$

where $c_1^2 = \left(\frac{\lambda+2\mu}{\rho}\right)$ and $\omega_1 = \left(\frac{\rho C_e c_1^2}{K^*}\right)$.

The equations (2.1), (2.2), (2.3), and (2.4) by taking into account (3.2) reduce to dimensionless form (after omitting the primes) as

$$a_1\frac{\partial e}{\partial r} + a_2\left(\nabla^2 u_r - \frac{u_r}{r^2}\right) - a_3\frac{\partial T}{\partial r} = \left(1 - \xi_1^2\nabla^2\right)\frac{\partial^2 u_r}{\partial t^2}, \tag{3.3}$$

$$a_1\frac{\partial e}{\partial z} + a_2\left(\nabla^2 u_z\right) - a_3\frac{\partial T}{\partial z} = \left(1 - \xi_1^2\nabla^2\right)\frac{\partial^2 u_z}{\partial t^2}, \tag{3.4}$$

$$\left(1 + \frac{\tau_0^\alpha}{\alpha!}\frac{\partial^\alpha}{\partial t^\alpha}\right)\left[\frac{\partial^2 T}{\partial t^2} + a_4\frac{\partial^2 e}{\partial t^2}\right] = \left(a_5 + \frac{\partial}{\partial t}\right)\nabla^2\phi, \tag{3.5}$$

$$\ddot{\phi} - \ddot{T} = \beta^*\nabla^2\phi, \tag{3.6}$$

$$t_{zz} = a_6\frac{\partial u_z}{\partial z} + a_7\left(\frac{1}{r}u_r + \frac{\partial u_r}{\partial r}\right) - \beta_1 T, \tag{3.7}$$

$$t_{zr} = a_8\left(\frac{\partial u_z}{\partial r} + \frac{\partial u_r}{\partial z}\right), \tag{3.8}$$

where a_i, $i = (1-8)$ are given in Appendix-I.

The displacement components u_r and u_z are expressed in terms of potential functions as

$$u_r = \frac{\partial q}{\partial r} + \frac{\partial^2\psi}{\partial r\,\partial z}, \qquad u_z = \frac{\partial q}{\partial z} - \left(\nabla^2 - \frac{\partial^2}{\partial z^2}\right)\psi. \tag{3.9}$$

Laplace and Hankel transforms are taken as

$$\left.\begin{aligned} \widehat{f}(r, z, s) &= \int_0^\infty e^{-st} f(r, z, t)\,dt \\ \widetilde{f}(\xi, z, s) &= \int_0^\infty \widehat{f}(r, z, s)\, r\, J_n(\xi r)\,dr \end{aligned}\right\}, \tag{3.10}$$

where Laplace transform parameter is s, Hankel transform parameter is ξ and J_n is Bessel function of first kind of order n.

Applying Laplace Transform and Hankel Transform on equation (3.6), we get

$$\widehat{T} = \widehat{\phi} - \varsigma\left(\frac{d^2}{dz^2} - \xi^2\right)\widehat{\phi}$$

where

$$\varsigma = \begin{cases} 0, & \text{for 1T}, \\ a, & \text{for 2T}, \\ \dfrac{\beta^*}{s^2}, & \text{for HTT}. \end{cases} \tag{3.11}$$

Equations (3.3), (3.4), (3.5), and (3.6) in the accompany of (3.9) and (3.10) yield the resulting expressions (suppressing the primes for convenience), after some algebraic calculations, we get

$$\left(L_1\frac{d^4}{dz^4} + L_2\frac{d^2}{dz^2} + L_3\right)(\tilde{q}, \tilde{\phi}) = 0, \tag{3.12}$$

$$\left(\frac{d^2}{dz^2} - \lambda_3^2\right)\widetilde{\psi} = 0, \tag{3.13}$$

where L_i, $i = 1$–3, λ_3 are defined in Appendix-II.

The roots of characteristic equations (3.12) and (3.13) are $\pm\lambda_i$, $i = 1, 2$ and λ_3, and the bounded solution can be expressed as

$$\begin{cases} \widehat{q} = A_1 e^{-\lambda_1 z} + A_2 e^{-\lambda_2 z}, \\ \widehat{\widetilde{\phi}} = d_1 A_1 e^{-\lambda_1 z} + d_2 A_2 e^{-\lambda_2 z}, \\ \widehat{\psi} = A_3 e^{-\lambda_3 z}. \end{cases} \tag{3.14}$$

where d_i $(i = 1, 2)$ are coupling constants, defined as

$$d_i = -\frac{\lambda_i^2 R_1 - R_2}{R_3 + R_4\lambda_i^2}, \qquad i = 1, 2.$$

Using the equations defined by (3.14) in the relations (3.3), (3.4), (3.5), (3.6), (3.7), and (3.8), along with (3.10), we obtain the following expressions

$$\widehat{u_r} = (-\xi)\sum_{i=1}^{2} A_i e^{-\lambda_i z} + \lambda_3 \xi A_3 e^{-\lambda_3 z}, \tag{3.15}$$

$$\widehat{u_z} = -\sum_{i=1}^{2} A_i e^{-\lambda_i z} + \xi^2 A_3 e^{-\lambda_3 z}, \tag{3.16}$$

$$\widehat{t_{zz}} = \sum_{i=1}^{3} H_i A_i e^{-\lambda_i z}, \tag{3.17}$$

$$\widehat{t_{zz}} = \sum_{i=1}^{3} H_{i+3} A_i e^{-\lambda_i z}, \tag{3.18}$$

$$\widehat{\phi} = \sum_{i=1}^{2} d_i A_i e^{-\lambda_i z}, \tag{3.19}$$

$$\widehat{T} = \sum_{i=1}^{2} H_{i+6} A_i e^{-\lambda_i z}, \tag{3.20}$$

4. BOUNDARY CONDITIONS

A circular thermal load is prescribed on the boundary surface $z = 0$. The source originates at $r = 0$ and expands radially over the surface with constant speed c. The bounding surface is assumed to be mechanically traction-free; hence, both the normal stress and tangential stress vanish at $z = 0$.

Mathematically these can be written as

$$\left.\begin{array}{ll} \text{(i)} & t_{zz} = 0, \\ \text{(ii)} & t_{zr} = 0, \\ \text{(iii)} & \phi = F_1 \dfrac{\delta(\mathrm{ct} - r)\, e^{\iota\omega t}}{2\pi r}, \end{array}\right\} \quad \text{at } z = 0. \tag{4.1}$$

Here δ is the Dirac delta function represents the localized nature of the expanding circular source, F_1 is the prescribed boundary-temperature intensity, c is the radial expansion speed of the circular source and ω is the frequency parameter.

Using (3.10) in (4.1), we have

$$\left.\begin{array}{ll} \text{(i)} & \widehat{\mathrm{t}_{zz}} = 0, \\ \text{(ii)} & \widehat{\mathrm{t}_{zr}} = 0, \\ \text{(iii)} & \widehat{\phi} = \dfrac{F_1}{2\pi} \dfrac{1}{\sqrt{\xi^2 - \frac{\omega^2}{c^2}}} e^{\iota\omega t}, \end{array}\right\} \quad \text{at } z = 0. \tag{4.2}$$

Making use of equations (3.15), (3.16), (3.17), (3.18), (3.19), and (3.20), in the boundary condition (4.2), we get the matrix formulation as $AX = B$,

where

$$A = \begin{bmatrix} H_1 & H_2 & H_3 \\ H_4 & H_5 & H_6 \\ d_1 & d_2 & 0 \end{bmatrix}, \qquad X = \begin{bmatrix} A_1 \\ A_2 \\ A_3 \end{bmatrix}, \qquad B = \begin{bmatrix} F_1 \\ 0 \\ 0 \end{bmatrix} \qquad \text{and} \qquad \Delta = \begin{vmatrix} H_1 & H_2 & H_3 \\ H_4 & H_5 & H_6 \\ d_1 & d_2 & 0 \end{vmatrix}.$$

The constants A_i are obtained from

$$A_i = \frac{\Delta_i}{\Delta}, \qquad i = 1, 2, 3. \tag{4.3}$$

where Δ_i $(i = 1, 2, 3)$ is obtained from Δ by replacing its i-th column with the vector $\begin{bmatrix}0 & 0 & \widetilde{F}_1\end{bmatrix}^T$.

Invoking (3.15), (3.16), (3.17), (3.18), (3.19), and (3.20), along with (4.3) give the transformed expression for different field quantities.

$$\widehat{u}_r = \frac{F_{10}}{\Delta}\left(\xi\left[-\sum_{i=1}^{2}\Delta_i e^{-\lambda_i z} + \lambda_3\Delta_3 e^{-\lambda_3 z}\right]\right), \tag{4.4}$$

$$\widehat{u}_z = \frac{F_{10}}{\Delta}\left(\left[-\sum_{i=1}^{2}\lambda_i\Delta_i e^{-\lambda_i z} + \xi^2\Delta_3 e^{-\lambda_3 z}\right]\right), \tag{4.5}$$

$$\widehat{t}_{zz} = \frac{F_{10}}{\Delta}\left[\sum_{i=1}^{3}H_i\Delta_i e^{-\lambda_i z}\right], \tag{4.6}$$

$$\widehat{t}_{zr} = \frac{F_{10}}{\Delta}\left[\sum_{i=1}^{3}H_{i+3}\Delta_i e^{-\lambda_i z}\right], \tag{4.7}$$

$$\widehat{\phi} = \frac{F_{10}}{\Delta}\left[\sum_{i=1}^{2}d_i\Delta_i e^{-\lambda_i z}\right], \tag{4.8}$$

$$\widehat{T} = \frac{F_{10}}{\Delta}\left[(H_7 + H_8)\Delta_1 e^{-\lambda_1 z} + (H_9 + H_{10})\Delta_2 e^{-\lambda_2 z}\right], \tag{4.9}$$

where all Δ_{ij} $(i = 1, 2, 3;\ j = 1, 2)$ and H_i $(i = 1, \ldots, 10)$ are defined in Appendix III.

5. SPECIAL CASES

- Let $\xi_1 \to 0$ in equations (4.4), (4.5), (4.6), (4.7), (4.8), and(4.9), determine the resulting expressions for visco-thermoelastic under MGT with HTT and fractional order derivative.
- By Substituting $K_1 = 0$ in equations (4.4), (4.5), (4.6), (4.7), (4.8), and(4.9), give the expressions of visco-thermoelastic under Lord-Shulman with non-local, HTT for fractional order.
- The desired expression for visco-thermoelastic Green-Naghdi-II (GN-II) model for fractional order are recovered by letting $K^* = \tau_0^\alpha = 0$, $K_1 > 0$ in equations (4.4), (4.5), (4.6), (4.7), (4.8), and(4.9).
- Resulting expression for visco-thermoelastic Green-Naghdi-III (GN-III) model with HTT for fractional order are given by letting $\tau_0^\alpha = 0$ in equations (4.4), (4.5), (4.6), (4.7), (4.8), and(4.9).

5.1. Sub Cases

i) if $\varsigma = a$: In equations (4.4), (4.5), (4.6), (4.7), (4.8), and(4.9), we obtain the results for visco-thermoelastic MGT with two temperatures along with non-local effect under fractional order derivatives.
ii) If $\varsigma = 0$: In equations (4.4), (4.5), (4.6), (4.7), (4.8), and(4.9), We attain the results for visco-thermoelastic MGT with one temperature along with non-local effect with fractional order derivatives.

6. INVERSION OF THE TRANSFORMS

The components of displacement, stresses, conductive temperature and temperature distribution are the functions of 's' and 'ξ' which are parameters of Laplace transform and Hankel transform respectively. To invert these quantities into physical domain, we invert the transforms by applying the method explained by Miglani and Kaushal [18].

7. NUMERICAL RESULT AND DISCUSSION

Following Dhaliwal and Singh [7], the numerical constants are chosen as
$\lambda = 2.17 \times 10^{10}$ Nm^{-2}, $\mu = 3.278 \times 10^{10}$ Nm^{-2}, $K^* = 1.7 \times 10^2$ Wm^{-1} deg^{-1},
$\omega_1 = 3.58 \times 10^{11}$ S^{-1}, $\beta_1 = 2.68 \times 10^6$ Nm^{-2} deg^{-1}, $\rho = 1.74 \times 10^3$ Kgm^{-3},
$C_e = 1.04 \times 10^3$ JKg^{-1} deg^{-1}, $T_0 = 298$ K. The nondimensional relaxation time and radial interval are taken as $\tau_0 = 0.3$ and $0 \leq r \leq 3$, respectively. For viscous cases, $Q_1 = 0.4$ and $Q_2 = 0.3$ are used.
Case I: Nonlocality and viscosity (Figures 1, 2, 3, and 4). With HTT= 0.75 and $\alpha = 0.5$ fixed, $\xi_1 = 0.75$ and $\xi_1 = 0$ are compared in viscous and non-viscous media. The labels VNL and VANL denote nonlocal and local viscous responses, respectively, whereas WVNL and WVANL denote nonlocal and local non-viscous responses, respectively.
Case II: HTT and viscosity (Figures. 5, 6, 7, and 8). With $\xi_1 = 0.75$ and $\alpha = 0.5$ fixed, HTT= 0.75 is compared with HTT= 0 in both viscous and non-viscous media. The labels VHT and VAHT denote viscous responses with and without HTT, respectively, whereas WVHT and WVAHT denote the corresponding non-viscous responses.
Case III: FOD parameter α (Figures 9, 10, 11, and 12). With $\xi_1 = 0.75$, HTT= 0.75 and the viscous parameters specified above, α is varied as 0.5, 0.7 and 1 to examine the fractional-order effect. The curves for $\alpha = 0.5$, $\alpha = 0.7$ and $\alpha = 1$ are represented by solid black, dotted red and dashed blue lines, respectively.

Case I: Non-local and Viscosity parameter

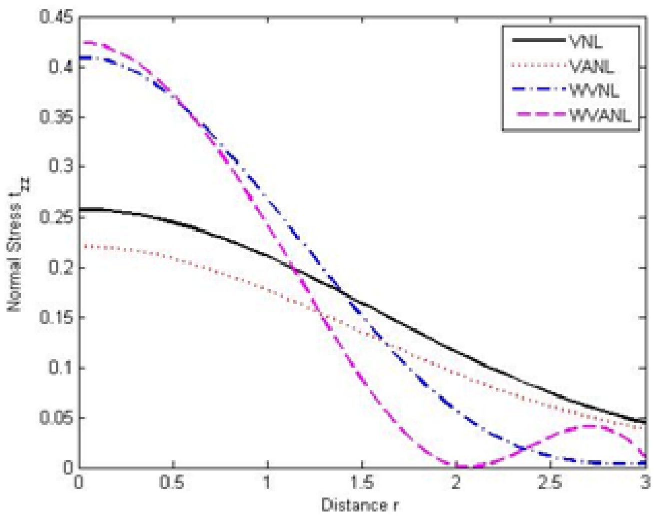

Figure 1. Profile of t_{zz} vs. r

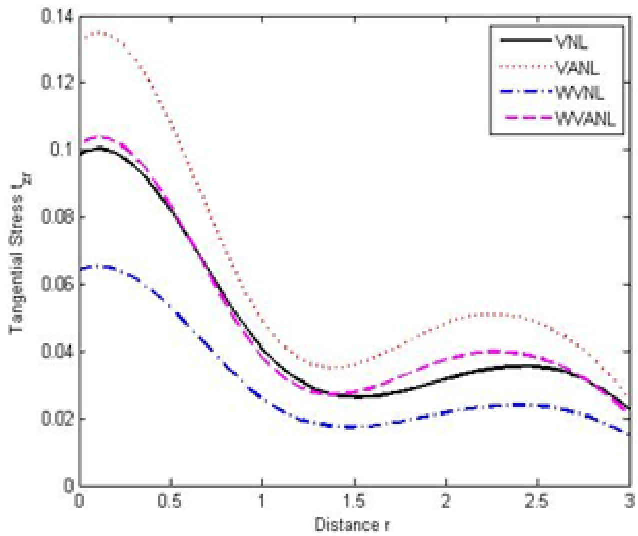

Figure 2. Profile of t_{zr} vs. r

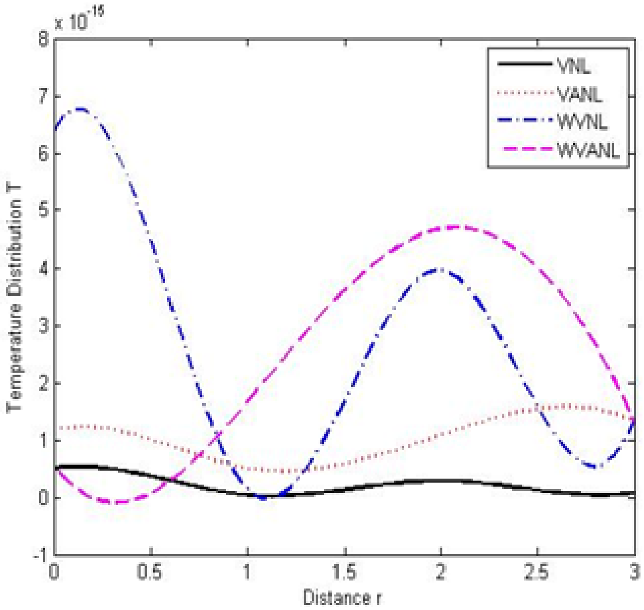

Figure 3. Profile of T vs. r

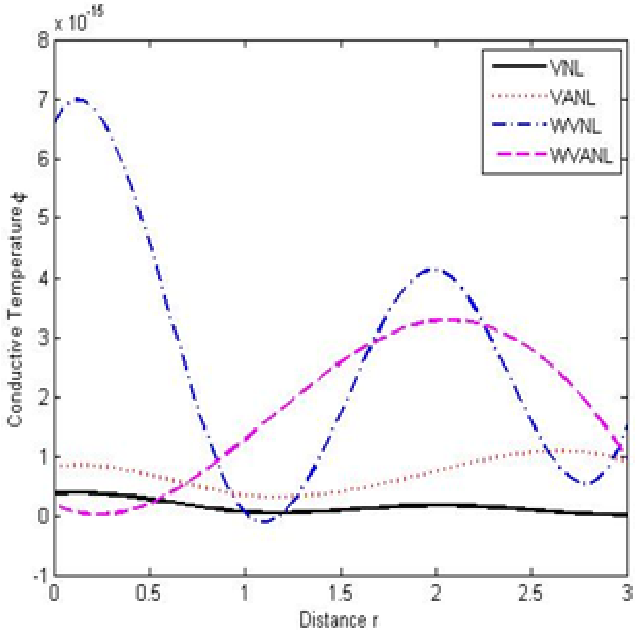

Figure 4. Profile of ϕ vs. r

Figure 1 depicts the variation of t_{zz} versus r. Near the loading surface, values of t_{zz} decreases for all the considered case. Moreover, the magnitude of t_{zz} is greater for VNL in comparison to VANL which reveals the impact of non-local parameter in presence of viscosity on the value of t_{zz}. Figure 2 depicts trend of t_{zr} versus r. It is noticed that near the loading surface, the magnitude of t_{zz} increases for all considered cases. As r increases, the magnitude of t_{zz} follows an decreasing behavior for all cases upto $r = 1.5$, further magnitude of t_{zz} become steady. Moreover, the values of t_{zr} remain on higher side for curve corresponding to case VANL than other considered cases. Figure 3 shows trend of T vs. r. It is noticed that the magnitude of T corresponding to curve WVNL While opposite behaviour is observed for the curve corresponding to WVANL. Also curve corresponding to VANL and VNL shows similar steady behaviour. Moreover, the value of T is greater for curve corresponding to WVNL in comparison to other considered curves which reveals non-local parameter has increasing effect on T. Figure 4 depicts the trend of ϕ vs. r. The value ϕ follows oscillatory behaviour for curve corresponding to VANL while similar steady behaviour is observed for VANL and VNL. Moreover, greater value of ϕ is noticed for curve corresponding to WVNL as compared to other considered case.

Case II: Impact of HTT and Viscosity

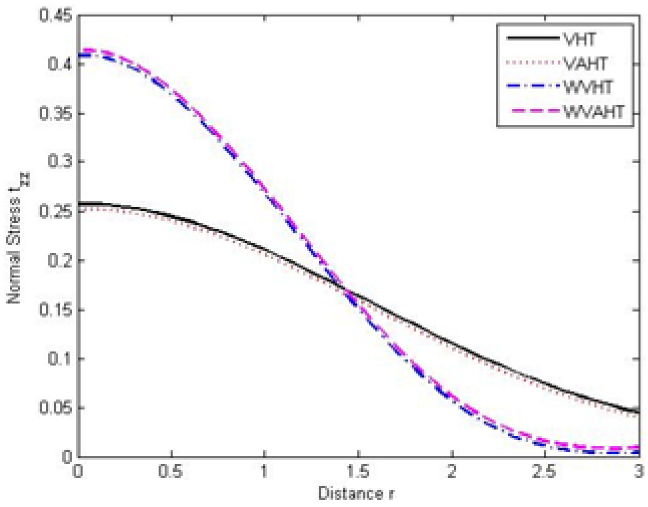

Figure 5. Profile of t_{zz} vs. r

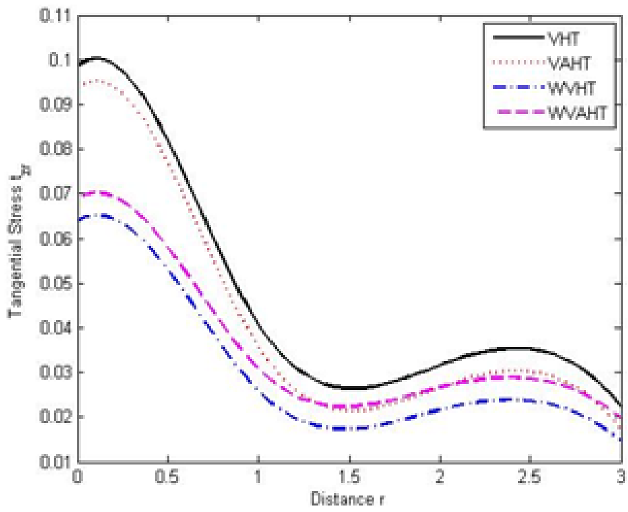

Figure 6. Profile of t_{zr} vs. r

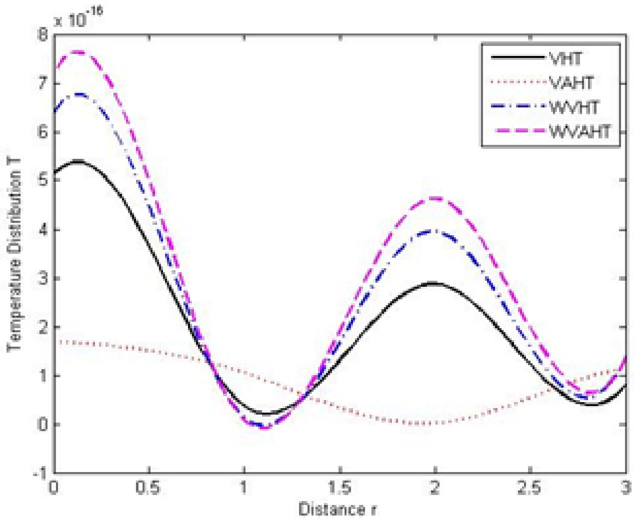

Figure 7. Profile of T vs. r

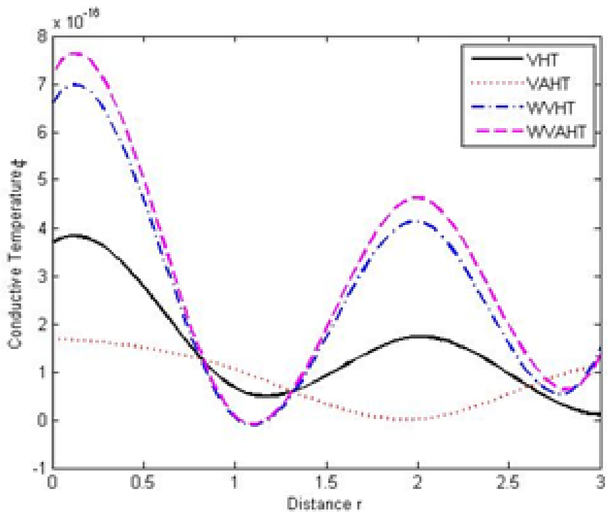

Figure 8. Profile of ϕ vs. r

Figure 5 depicts the variations of t_{zz} vs. r. It is noticed that near the loading surface, the magnitude of t_{zz} shows similar decreasing pattern for all considered cases, it is noticed that curve corresponding to WVAHT is on higher side for $0 \leq r \leq 1.5$ while for $r \geq 1.5$ the curve corresponding to VHT is on higher side in comparison to other considered cases. Figure 6 shows variations of t_{zr} vs. r. It is evident that t_{zr} follows a similar oscillatory pattern for all the considered cases but magnitude of t_{zz} is on higher side for curve corresponding to VHT. Figure 7 shows the variations of T vs. r. It is noticed that the magnitude of T depicts similar oscillatory behavior for all considered curves. The magnitude of variations is noticed on higher side for curve corresponding to VAHT. The plot of ϕ vs. r is illustrated in figure 8. It is noted that values of ϕ exhibit a similar oscillatory pattern across all considered curves except for the curve corresponding to VAHT but magnitude of ϕ is higher for WVAHT when compared with all other considered curves.

Case III: Effect of FOD

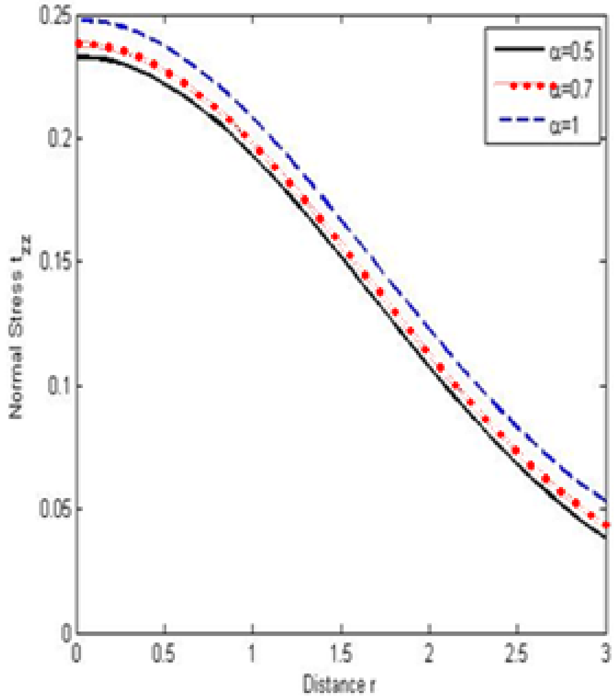

Figure 9. Profile of t_{zz} vs. r

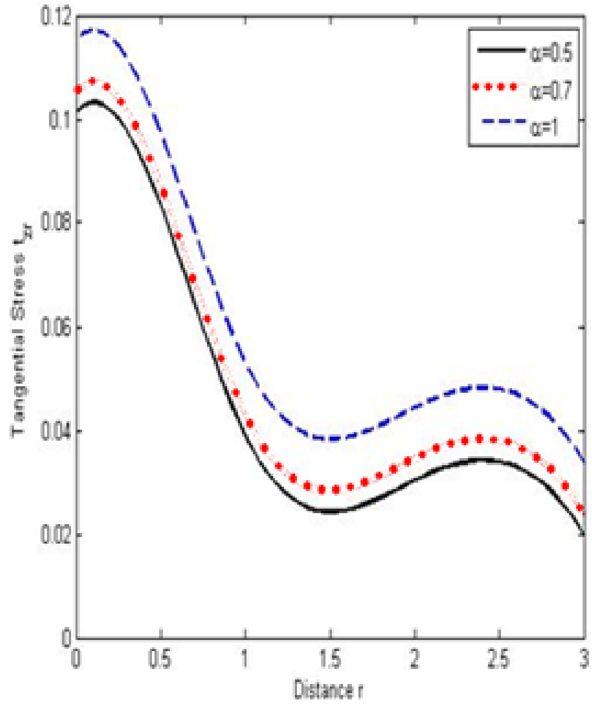

Figure 10. Profile of t_{zr} vs. r

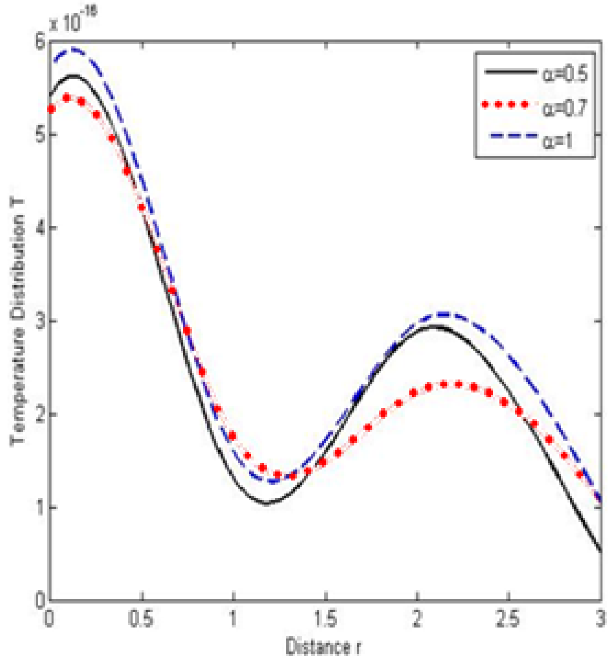

Figure 11. Profile of T vs. r

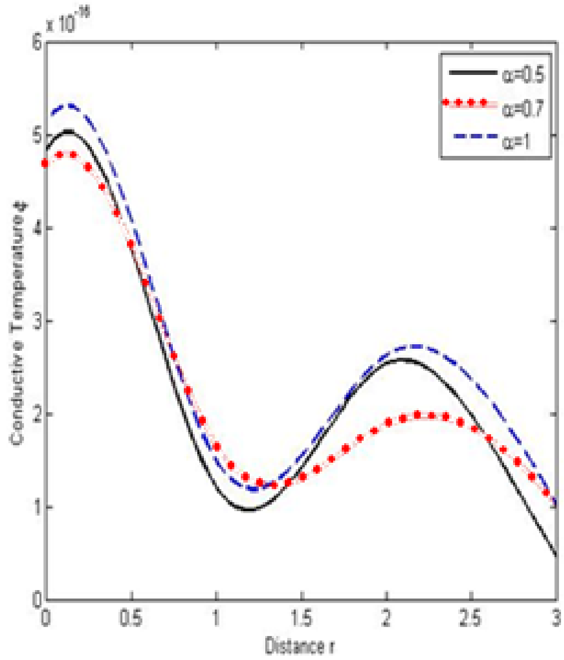

Figure 12. Profile of ϕ vs. r

Figure 9 shows the variation of t_{zz} with r. The normal stress t_{zz} behaves as a continuously decreasing function of r. It has the maximum value near the boundary and gradually decreases as the distance increases. This shows that the normal stress is more concentrated near the loaded surface and becomes weaker away from the source. As α changes from 0.5 to 1, the separation between the curves becomes clear, with larger α producing a stronger response throughout the region. This indicates that the fractional-order parameter directly affects the intensity and decay rate of the normal stress field. Figure 10 represents the behavior of t_{zr} with r. t_{zr} first decreases sharply from the boundary and reaches a minimum at an intermediate distance. After that, it increases slightly to form a secondary peak and then decreases again near the outer region. The influence of α is visible over the whole range, since larger values maintain a higher shear-stress level, whereas smaller values reduce the amplitude of t_{zr}. Figure 11 shows the variation of T with r. T is high near the boundary and decreases rapidly as r increases. It reaches a minimum at an intermediate distance, then rises again to a secondary maximum, and finally decreases toward the outer region. For higher values of α, the thermal disturbance is transmitted more effectively, giving a larger temperature distribution. Lower values of α suppress the temperature field because of stronger memory and damping effects. Figure 12 illustrates the variation of ϕ with radial distance r. ϕ behaves almost similarly to the temperature distribution T. It starts with a high value near the boundary, decreases to a minimum at an intermediate distance, then increases to a secondary maximum and finally decreases again. The effect of α is also significant, because increasing α enhances conductive heat transfer, while smaller values produce a weaker and more damped conductive-temperature response.

8. CONCLUSION

An axisymmetric source problem in a visco-thermoelastic half-space has been studied under the MGT heat equation with HTT, nonlocal, viscosity and FOD effects. The problem is driven by a circular thermal source acting on the boundary surface, while the mechanical boundary is traction-free. By using potential functions along with Laplace and Hankel transforms, the displacement components, stress components, conductive temperature and thermodynamic temperature are obtained in the transformed domain and evaluated numerically after inversion.

The numerical results show that the nonlocal parameter, HTT parameter, viscosity and fractional-order parameter significantly influence the response of the medium under thermal loading. The nonlocal parameter modifies the stress and temperature distributions by incorporating small-scale interactions. Viscosity changes the magnitude of the field quantities and introduces damping into the response. The HTT parameter affects the relation between conductive and thermodynamic temperatures, confirming the importance of using two distinct temperature fields. The fractional-order parameter α controls the memory-dependent behavior of the medium; increasing α generally enhances the stress and temperature amplitudes, whereas smaller values produce a more attenuated response.

The proposed formulation is sufficiently general to include several special cases, such as the one-temperature model and other reduced thermoelastic models obtained by suitable choices of the parameters. The results may be useful for the analysis of advanced materials, layered structures, geophysical media and engineering components subjected to localized thermal loading over circular.

Conflict of Interest

The authors declare there is no existing conflict of interest.

Appendix-I

$$a_1 = \frac{\lambda + \mu}{\rho c_1^2}, \quad a_2 = \frac{\mu}{\rho c_1^2}, \quad a_3 = \frac{\beta_1 T_0}{\rho c_1^2}, \quad a_4 = \frac{\beta_1 c_1}{K^*}, \quad a_5 = \frac{K_1}{K^* \omega_1},$$
$$a_6 = \frac{\lambda + 2\mu}{\beta_1 T_0}, \quad a_7 = \frac{\lambda}{\beta_1 T_0}, \quad a_8 = \frac{\mu}{\beta_1 T_0}, \quad \nabla^2 = \frac{\partial^2}{\partial r^2} + \frac{1}{r}\frac{\partial}{\partial r} + \frac{\partial^2}{\partial z^2}.$$

Appendix-II

$$L_1 = R_4 R_6 - R_1 R_9, \quad L_2 = R_1 R_8 + R_2 R_9 + R_3 R_6 + R_4 R_{10}, \quad L_3 = R_3 R_{10} - R_2 R_8,$$
$$\lambda_3 = \frac{R_{11}}{R_{12}}, \quad R_1 = 1 + \xi^2 s^2, \quad R_2 = \xi^2 + (1 + \xi^2)\xi_1^2 s^2, \quad R_3 = a_3(1 + \varsigma\xi^2), \quad R_4 = a_3\varsigma,$$
$$R_5 = s^2\left(1 + \frac{\tau_0^\alpha}{\alpha!}s^\alpha\right), \quad R_6 = \left(1 + \frac{\tau_0^\alpha}{\alpha!}s^\alpha\right)a_4 s, \quad R_7 = a_5 + s,$$
$$R_8 = R_5(1 + \varsigma\xi^2) + R_7\xi^2, \quad R_9 = R_5\varsigma + R_7, \quad R_{10} = -R_6\xi^2,$$
$$R_{11} = a_2\xi^2 + (1 + \xi^2)\xi_1^2 s^2, \quad R_{12} = \xi_1^2 s^2.$$

Appendix-III

$$\Delta = d_1(H_2H_6 - H_3H_5) + d_2(H_3H_4 - H_1H_6), \quad \Delta_2 = H_3H_4 - H_1H_6, \quad \Delta_1 = H_2H_6 - H_3H_5,$$
$$\Delta_3 = H_1H_5 - H_2H_4, \quad \Delta_{31} = d_2H_4 - d_1H_5,$$
$$H_i = a_6\lambda_i^2 - a_7\xi^2 - (1 + \varsigma\xi^2)d_i + \varsigma d_i\lambda_i^2, \quad H_3 = \lambda_3\xi^2(a_7 - a_6),$$
$$H_{i+3} = 2\lambda_i\xi a_8, \quad H_6 = \xi a_8(\lambda_3^2 + \xi^2), \quad H_{i+6} = (1 + \varsigma\xi^2)d_i + \varsigma d_i\lambda_i^2,$$
$$H_9 = (1 + \varsigma\xi^2)d_2, \quad H_{10} = -\varsigma d_2\lambda_2^2.$$

References

1. Abouelregal, A. E. (2020). A novel model of nonlocal thermoelasticity with time derivatives of higher order. *Mathematical Methods in the Applied Sciences*.
2. Abouelregal, A. E., Ahmad, H., Badr, S., Almutairi, B., and Almohsen, B. (2022). Viscoelastic stressed microbeam analysis based on moore-gibson-thompson heat equation and laser excitation resting on winkler foundation. *Journal of Low Frequency Noise, Vibration and Active Control*, 41:1–22.
3. Abouelregal, A. E., Akgoz, B., and Civalek, O. (2023). Magneto-thermoelastic interactions in an unbounded orthotropic viscoelastic solid under the Hall current effect by the fourth-order Moore-Gibson-Thompson equation. *Computers & Mathematics with Applications*, 141:102–115.

4. Alzahrani, F. S. and Abbas, I. A. (2020). Photo-thermal interactions in a semiconducting media with a spherical cavity under hyperbolic two-temperature model. *Mathematics*, 8(4):585.

5. Chen, P. J. and Gurtin, M. E. (1968). On a theory of heat conduction involving two temperatures. *Zeitschrift für Angewandte Mathematik und Physik*, 19(4):614–627.

6. Chen, P. J., Gurtin, M. E., and Williams, W. O. (1969). On the thermoelastic material with two temperatures. *Zeitschrift für Angewandte Mathematik und Physik*, 20:107–112.

7. Dhaliwal, R. S. and Singh, A. (1980). *Dynamic Coupled Thermoelasticity*. Hindustan Publishing Corporation, New Delhi.

8. El-Bary, A. A. (2021). Diagonalization method to hyperbolic two-temperature generalized thermoelastic solid sphere under mechanical damage effect. *Crystals*, 11(9).

9. Eringen, A. C. and Edelen, D. G. B. (1972). On non-local elasticity. *International Journal of Engineering Science*, 10(3):233–248.

10. Ezzat, M. A., El-Karamany, A. S., El-Bary, A. A., and Fayik, M. A. (2013). Fractional calculus in one-dimensional isotropic thermo-viscoelasticity. *Comptes Rendus Mécanique*, 341(7):553–566.

11. Ezzat, M. A., El-Karamany, A. S., Samaan, A. A., and Zakaria, M. (2003). The relaxation effects of the volume properties of viscoelastic material in generalized thermoelasticity with thermal relaxation. *Journal of Thermal Stresses*, 26(7):671–690.

12. Green, A. E. and Lindsay, K. A. (1972). Thermoelasticity. *Journal of Elasticity*, 2:1–7.

13. Hilal, M. I., Tantawi, R., Elshazly, I. S., Bachar, I., Sharma, S., and Lotfy, K. (2025). Thermomechanical waves in magnetized microelongated thermoelastic medium using the Moore-Gibson-Thompson model. *AIP Advances*, 15:035343.

14. Lord, H. W. and Shulman, Y. (1967). A generalized dynamical theory of thermoelasticity. *Journal of the Mechanics and Physics of Solids*, 15(5):299–309.

15. Lotfy, K., Elshazly, I. S., Bachar, I., Sharma, S., El-Bary, A. A., and Yaseen, N. A. (2025a). Fractional photo-thermoelastic waves of hydrodynamic semiconductors with Hall currents and variable thermal conductivity. *Case Studies in Thermal Engineering*, 71:106180.

16. Lotfy, K., Elshazly, I. S., Halouani, B., Sharma, S., and Elidy, E. S. (2025b). Piezo-photothermal wave dynamics in an orthotropic hygrothermal semiconductor exposed to heat and moisture flux. *European Physical Journal B*, 98:9.

17. Marin, M., Ochsner, A., and Bhatti, M. M. (2020). Some results in moore-gibson-thompson thermoelasticity of dipolar bodies. *Journal of Applied Mathematics and Mechanics*, 100.

18. Miglani, A. and Kaushal, S. (2011). Axi-symmetric deformation in generalized thermoelasticity with two temperatures. *Arabian Journal for Science and Engineering*, 36:1581–1595.

19. Quintanilla, R. (2019). Moore-gibson-thompson thermoelasticity. *Mathematics and Mechanics of Solids*, 24:4020–4031.

20. Saeed, T. and Abbas, I. (2022). Effects of the non-local thermoelastic model in a thermoelastic nanoscale material. *Mathematics*, 10(2):284.

21. Sharma, S. (2024). The effect of the impedance limit on the reflection of plane waves in a micropolar thermoviscoelastic material using a modified Green-Lindsay model. *Romanian Journal of Acoustics and Vibration*, 21(2):199–209.

22. Sharma, S. (2025). An examination of the fundamental solution and Green's function in orthotropic photothermoelastic with diffusion under the MGT model. *Analele Ştiinţifice ale Universităţii Ovidius Constanţa, Seria Matematică*, 33(3):165–213.

23. Sharma, S. and Khator, S. (2021). Power generation planning with reserve dispatch and weather uncertainties including penetration of renewable sources. *International Journal of Smart Grid and Clean Energy*, 10(4):292–303.

24. Sharma, S. and Khator, S. (2022). Micro-grid planning with aggregator's role in the renewable inclusive prosumer market. *Journal of Power and Energy Engineering*, 10(4).

25. Youssef, H. M. (2006). Theory of two-temperature generalized thermoelasticity. *IMA Journal of Applied Mathematics*, 71(3):383–390.

26. Youssef, H. M. and El-Bary, A. A. (2018). Theory of hyperbolic two-temperature generalized thermoelasticity. *Materials Physics and Mechanics*, 40:158–171.

27. Youssef, H. M., El-Bary, A. A., and Al-Lehaibi, E. A. N. (2021). Thermal stress analysis of a damaged solid sphere using hyperbolic two-temperature generalized thermoelasticity theory. *Scientific Reports*, 11.

28. Yu, Y. J., Tian, X., and Xiong, Q. (2016). Nonlocal thermoelasticity based on nonlocal heat conduction and nonlocal elasticity. *European Journal of Mechanics – A/Solids*, 60:238–253.